iScience

CellPress
OPEN ACCESS

Article

Nuclear miR-150 enhances hepatic lipid accumulation by targeting RNA transcripts overlapping the *PLIN2* promoter

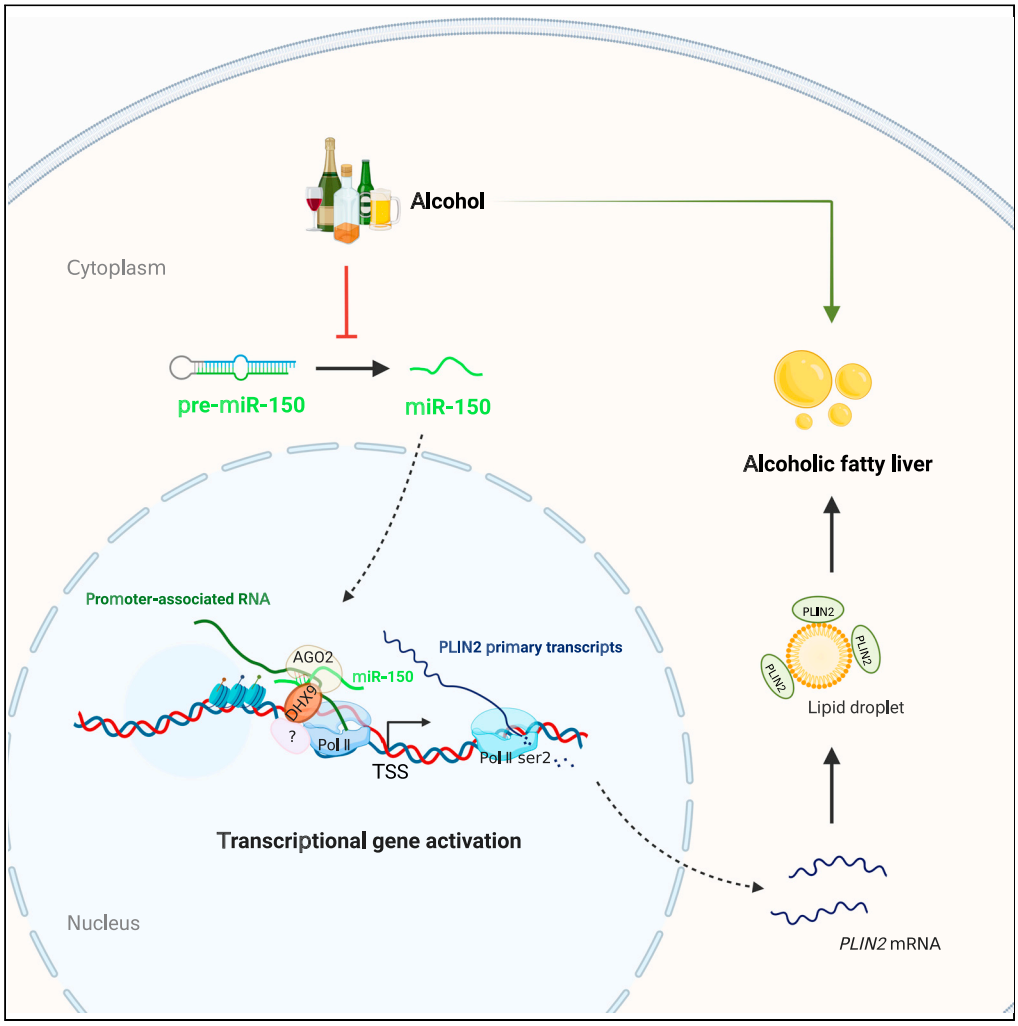

Jiao Luo, Yanan Ji, Ningning Chen, Ge Song, Shuyue Zhou, Xuan Niu, Dianke Yu

dianke.yu@qdu.edu.cn

Highlights

miR-150 downregulation was a compensatory response to ethanol-induced steatosis

miR-150 targets the promoter of *PLIN2*, a gene involves in lipid sequestration

miR-150 promotes PLIN2 expression by directly binding and stabilizing the pRNAs

miR-150 activates *PLIN2* transcription by facilitating RNAPII/DHX9 recruitment

Luo et al., iScience *26*, 107837
October 20, 2023
https://doi.org/10.1016/j.isci.2023.107837

iScience

CellPress
OPEN ACCESS

Article

Nuclear miR-150 enhances hepatic lipid accumulation by targeting RNA transcripts overlapping the *PLIN2* promoter

Jiao Luo,[1,2] Yanan Ji,[1,2] Ningning Chen,[1] Ge Song,[1] Shuyue Zhou,[1] Xuan Niu,[1] and Dianke Yu[1,3,*]

SUMMARY

Alcohol-associated liver disease is a prevalent chronic liver disease caused by excessive ethanol consumption. This study aims to investigate the role of miR-150 in regulating hepatic lipid homeostasis in alcoholic fatty liver (AFL). miR-150 was mainly distributed in the nucleus of hepatocytes and correlated with the degree of liver injury. The decreased expression of miR-150 observed in AFL was a compensatory response to ethanol-induced hepatic steatosis. Overexpression of miR-150 facilitated hepatic lipid accumulation *in cellulo* and exacerbated ethanol-induced liver steatosis *in vivo*. *In silico* analysis identified perilipin-2 (*PLIN2*) as a potential target gene of miR-150. miR-150 activated *PLIN2* transcription by directly binding the RNA transcripts overlapping *PLIN2* promoter and facilitating the recruitment of DNA helicase DHX9 and RNA polymeraseII. Overall, our study provides fresh insights into the homeostasis regulation of hepatic steatosis induced by ethanol and identifies miR-150 as a pro-steatosis effector driving transcriptional *PLIN2* gene activation.

INTRODUCTION

Alcohol-associated liver disease (ALD) is a prevalent chronic liver diseases caused by long-term and excessive ethanol drinking, which contributes significantly to liver-related morbidity and mortality worldwide.[1] More than 90% of heavy drinkers suffer from hepatic steatosis, an early stage of ALD manifested by lipid accumulation in the liver. Although abstinence can significantly ameliorate or reverse alcoholic fatty liver (AFL), few patients can successfully abstain from alcohol. Moreover, ALD can progress through simple steatosis to advanced hepatitis, liver fibrosis, cirrhosis, and even hepatocellular carcinoma.[2,3] The severity of liver steatosis is highly correlated with the development of later stages of ALD.[4] To date, considerable efforts have been made to explore the mechanisms underlying the pathogenesis of ALD.[5,6] Acetaldehyde and imbalanced redox state produced by ethanol metabolism are generally considered major contributors to the development and progression of ALD.[7,8] While the pathogenic factor of AFL is clear and definite, a better understanding of the mechanisms maintaining steatosis is essential for identifying early biomarkers and developing effective therapeutics for ALD.

The pathogenesis of alcoholic steatosis is a complex process. Excessive alcohol consumption has been reported to dramatically induce liver CD36 expression, which contributes to circulating fatty acid uptake.[9] Many responses of hepatocytes to fatty acids are modulated by SREBP1c and PPAR-α. Toxic acetaldehyde increases SREBP1c expression, which exerts adverse effect by promoting fatty acid biosynthesis,[10] whereas PPAR-α prevents ethanol-induced steatosis. However, chronic alcohol consumption or acetaldehyde impairs PPAR-α DNA binding activity, subsequentially inhibiting PPAR-α signaling.[11,12] Additionally, lipid droplet coat protein FSP27/Cidec[13,14] and Perilipin-2 (PLIN2)[15] are upregulated in alcohol-induced liver damage, which promote the formation of lipid droplets and triglyceride (TG) deposition. Ethanol exposure also decreases microsomal triglyceride transfer protein (MTTP), impairs very-low-density lipoprotein (VLDL) assembly and ultimately inhibits hepatic lipid export.[16] Consequentially, homeostasis disruption of the hepatic lipid metabolic process, including fatty acid uptake, esterification and oxidation, TG sequestration and export, etc., is closely related to the development of AFL.[17,18] However, the detailed molecular events that underlie the regulation of lipid homeostasis in ALD, such as the compensatory response, have not yet been fully characterized.

MicroRNAs (miRNAs) are a class of endogenous small noncoding RNAs that are approximately 22 nucleotides in length. Generally, miRNAs negatively regulate target gene expressions at post-transcriptional level by directly binding the 3′UTR sequence of cognate mRNA transcripts.[19] miRNAs are highly conserved across animals and human, and they participate in almost all biological process and disease development. Various miRNAs have been shown function in regulating the pathogenesis of ALD. For example, alcohol consumption has been shown to decrease miR-148a expression, which facilitates TXNIP overexpression and inducing hepatic pyroptosis.[20] Chronic ethanol exposure

[1]School of Public Health, Qingdao University, Qingdao, China
[2]The authors contributed equally
[3]Lead contact
*Correspondence: dianke.yu@qdu.edu.cn
https://doi.org/10.1016/j.isci.2023.107837

significantly induced miR-217 expressions, which promoting hepatic fat accumulation by downregulating SIRT1.[21] Additionally, *MiR-200c-KO* mice were resistant to the development of AFL by cooperatively promoting Hnf1b and ApoO functions and increasing TG secretion.[22]

Although miRNAs generally suppress gene expression by promoting mRNA degradation or inhibiting protein translation in the cytoplasm, increasing evidence suggests that particular miRNAs exist within the nucleus and can modulate transcriptional gene silencing (TGS) or transcriptional gene activation (TGA).[23] For example, nuclear miR-665 has been reported to aggravate heart failure by suppressing *PTEN* transcription.[24] Additionally, miR551b-3p has been found to interact with the *STAT3* promoter and activate *STAT3* transcription, leading to enhanced tumor growth.[25] Notably, miR-589 has been shown to act as a small activating miRNA that interacts with the RNA transcripts overlapping the *COX-2* promoter.[26] However, the nuclear functions of miRNAs in alcohol-induced liver injury are still not fully understood and require further investigation.

In this study, we examined the cellular distribution of miRNAs that were dysregulated in the AFL and found that decreased expression of nuclear miR-150 served as a compensatory response to ethanol-induced hepatic steatosis. Interestingly, contrary to conventional miRNA negative regulation, we discovered that miR-150 targeted RNA transcripts overlapping the *PLIN2* promoter, recruiting relevant transcription factors and facilitating the transcriptional activation of *PLIN2*.

RESULTS

Dysregulated miRNAs in AFL mouse liver: Focus on nuclear miR-150

We established an AFL disease mouse model using chronic-plus-binge ethanol feeding for 8 weeks (Figure 1A). To identify dysregulated miRNAs in this model, we performed small RNA sequencing on livers from ethanol-fed and pair-fed mice, and a total of 1,576 miRNAs were detected. Unsupervised clustering analysis grouped alcoholic mice and control samples separately, showing the difference in miRNA expressions between groups ($|\log_2 FC| > 0.58$ and $p < 0.05$). Specifically, 27 miRNAs were upregulated while 11 miRNAs were downregulated in ethanol-fed mice compared to pair-fed mice (Figure 1B). To validate these sequencing results, we assessed the hepatic expression of the 38 dysregulated miRNAs identified, using qRT-PCR. Finally, 24 miRNAs were identified significantly dysregulated in the liver of alcoholic mice (Figures 1C and 1D).

To exploring the subcellular distribution of these 24 dysregulated miRNAs, we purified the nuclear and cytoplasmic fractions from mouse hepatic cell line AML12 cells. The high purity of isolated compartments was confirmed by using the nuclear RNA marker *U6* small nuclear RNA and cytoplasmic RNA marker *GAPDH* (Figure 1E). qRT-PCR results showed that miR-150-5p, miR-154-5p, miR-1948-3p, miR-379-3p, miR-382-5p, miR-409-5p, miR-411-3p, miR-541-5p, and miR-802-3p had the highest signal, with more than 80% of the factions distributing in the nucleus. Considering the cellular expression levels and sequence conservation, miR-150 was selected as the candidate miRNA for further study (Table S1).

As shown in Figure 1F, miR-150 was found to be specifically and highly expressed in liver tissue. Further sequence comparison revealed that miR-150 was highly conserved among placental mammals, and possessed an AGUG nucleotide sequence at its 3′ end which may serve as a nuclear targeting motif (Figure 1G). To further validate the nuclear localization of miR-150, primary hepatocytes (PHC) were isolated from C57/BL6 mouse, and fluorescence *in situ* hybridization (FISH) was performed using Cy3-labled miRNA probes. As seen in Figure 1H, miR-150 was detected in the PHC nucleus that was heavily stained by DAPI. Taken together, our data suggest that miR-150 is mainly distributed in the nucleus of hepatic cell.

miR-150 is highly correlated with alcoholic liver injury

To investigate the expression patterns of miR-150 in the AFL mice, two additional ALD mice models were established by feeding male C57/BL6 mice ethanol diet for 10 days and 6 weeks-plus-one binge (E10d+1B, E6w+1B). Livers from mice chronically fed ethanol for 10 days or 6 weeks-plus-one binge appeared with micro-steatosis and demonstrated lower levels of liver injury than those fed ethanol for 8 weeks-plus-one binge (E8w+1B), as evidenced by H&E and Oil Red O staining (Figure 2A). The expression levels of pre-miR-150 remained unchanged in all chronical ethanol feeding models (Figure 2B), but mature miR-150 was significantly downregulated in the E10d+1B mice, and its expression levels further decreased with increasing ethanol feeding time (Figure 2C). PHC isolated from the AFL livers showed dramatic down-regulation of miR-150. Our data demonstrated that miR-150 was significantly decreased in the liver of AFL mice.

Intriguingly, a strong correlation was found between the reduced expression of miR-150 and the degree of liver injury, as indicated by serum alanine aminotransferase (ALT) levels (Figure 2E), and the correlation was stronger with the increasing alcohol consumption time. Similar results were observed from the close relation between miR-150 expressions and liver TG levels (Figure 2F). These results suggested that miR-150 might be an indicator of the degree of liver injury in AFL.

miR-150 enhances alcohol-induced hepatic lipid accumulation

miR-150 was decreased in the AFL (Figure 2C), an initial-stage ALD. The expression profiles of miR-150 in the livers of alcoholic hepatitis patients and alcoholic liver disease-induced cirrhosis individuals were retrieved form the GEO dataset GSE59492; however, we found that miR-150 was significantly upregulated in the liver tissues of advanced ALD (Figure 3A). *In cellulo* chronic EtOH exposure results showed that short-term ethanol exposure drastically decreased miR-150 expressions while long-term ethanol exposure profoundly elevated miR-150 levels (Figure 3B). Oil Red O staining showed that miR-150 mimics markedly enhanced the accumulation of hepatic lipids in AML12

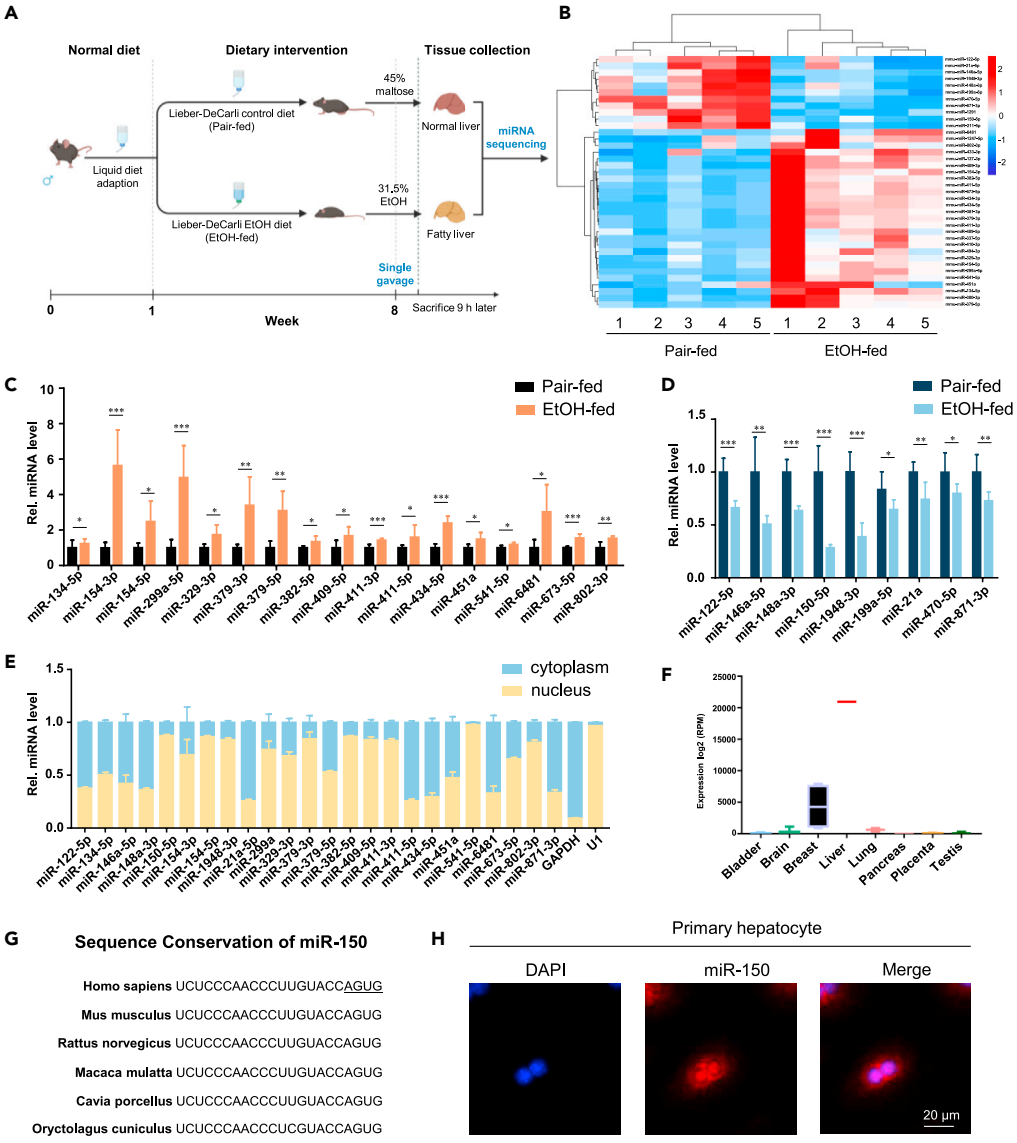

Figure 1. The cellular distribution of dysregulated miRNAs in the liver of alcoholic fatty liver (AFL) disease mice

(A) Schematic of AFL mice model by acute-on-chronic ethanol feeding. AFL mice were fed with Lieber-DeCarli liquid diet of 4% ethanol (w/w). After 8-week feeding, AFL mice were acutely administrated with 31.5% ethanol by oral gavage. Graph was created with BioRender.com.

(B) Heatmap of dysregulated miRNAs in the livers of AFL mice (n = 5) as compared with pair-fed controls (n = 5) (|log2FC| > 0.58, $p < 0.05$).

(C and D) Validation of upregulated (C) and downregulated (D) miRNAs in ethanol-fed mice livers by RT-qPCR analysis. Data was shown as mean ± SD. *$p < 0.05$, **$p < 0.01$, ***$p < 0.001$ as indicated.

(E) The cellular location of 24 validated dysregulated miRNAs in AML12 cells. miRNAs in the nuclear and cytoplasmic fractions were extracted, reverse-transcribed, and quantified by real-time PCR. Data was shown as mean ± SD.

(F) miR-150 expression levels in multiple human tissues. The expression profiles were retrieved from miRmine database. Data was shown as mean ± SD.

(G) Sequence alignment analysis of miR-150 from humans and other placental mammals.

(H) Cellular distribution of miR-150 in mouse primary hepatic cells by FISH analysis using Cy3-labeled microRNA Detection Probes. Scale bar, 20 μM.

and PHC (Figures 3C and 3E), while miR-150 inhibitors mitigated the basal level of the hepatic lipids (Figure S1). These data suggest that the decrease of miR-150 in AFL is a part of a compensatory response to ethanol-induced hepatic steatosis. Moreover, PHC treated with ethanol displayed prominent lipid accumulation; however, further inhibition of endogenous miR-150 by its inhibitor drastically attenuated ethanol-induced lipid accumulation (Figure 3F).

To clarify the functional role of miR-150 in alcoholic liver disease *in vivo*, we over-expressed miR-150 in AFL mice liver using a rAAV8 system for long-term effects (Figures 3G and 3H). miR-150 overexpression increased hepatic TG contents in ethanol-fed mice (Figure 3I) while serum

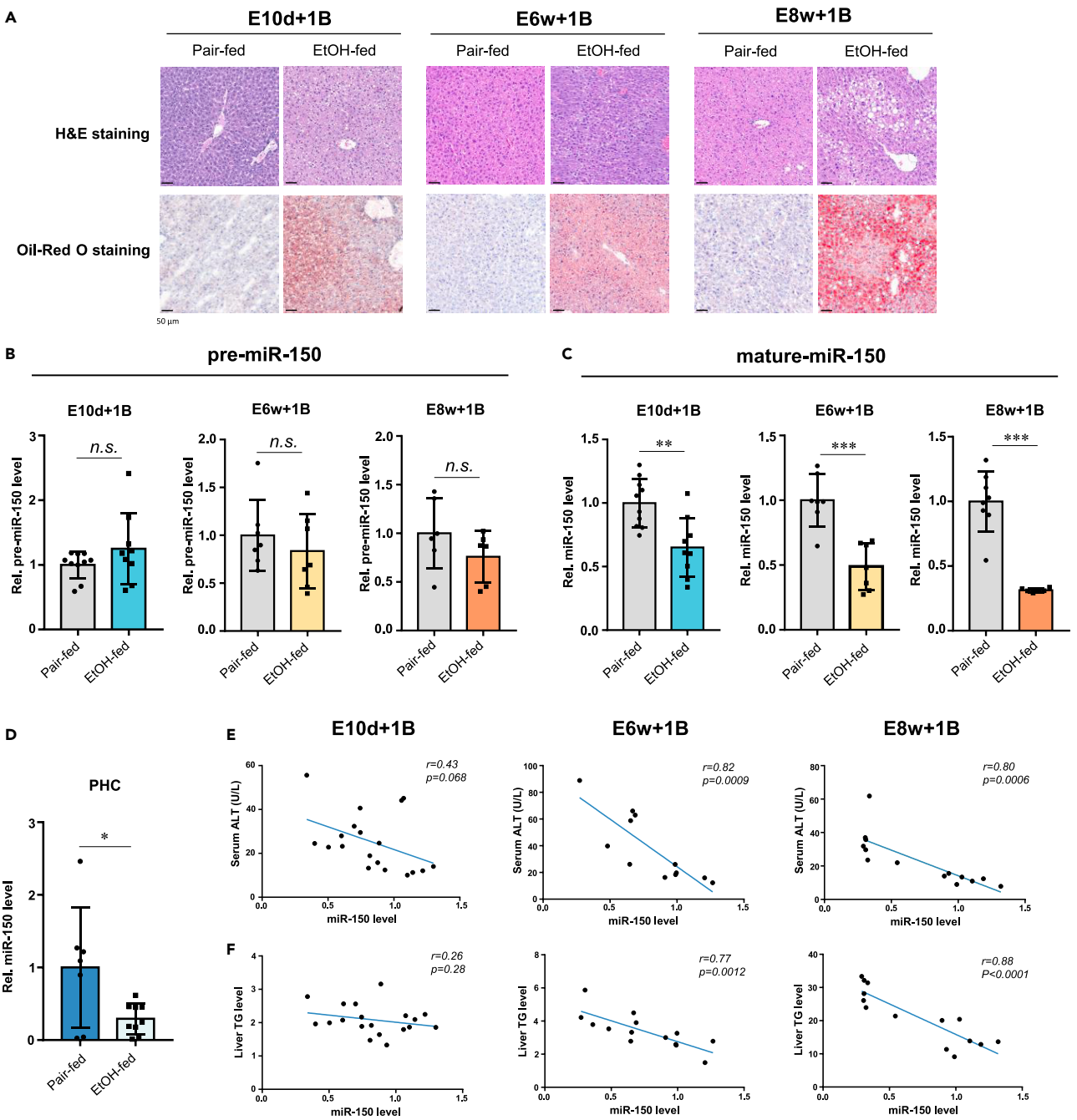

Figure 2. Liver miR-150 is decreased in the liver of AFL mice

(A) Liver H&E staining and Oil Red O staining of mice fed with 10-day, 6-week, or 8-week ethanol plus one binge and pair-fed mice. Scale bar, 50 μM.

(B and C) The liver expression levels of pre-miR-150 (B) and mature miR-150 (C) in mice fed with 10-day, 6-week, or 8-week ethanol plus one binge (E10d+1B, E6w+1B, or E8w+1B) and pair-fed mice. Data was shown as mean ± SD. *n.s.*, not significant; **p < 0.01, ***p < 0.001 as indicated.

(D) The liver expression levels of miR-150 in isolated primary hepatocytes from mice fed with 7-week ethanol plus one binge and pair-fed mice. Data was shown as mean ± SD. *p < 0.05.

(E) *Pearson* correlation analysis between miR-150 expression levels and serum ALT levels in E10d+1B, E6w+1B, and E8w+1B mice and corresponding pair-fed mice.

(F) *Pearson* correlation analysis between miR-150 expression levels and liver TG levels in E10d+1B, E6w+1B, and E8w+1B mice and corresponding pair-fed mice.

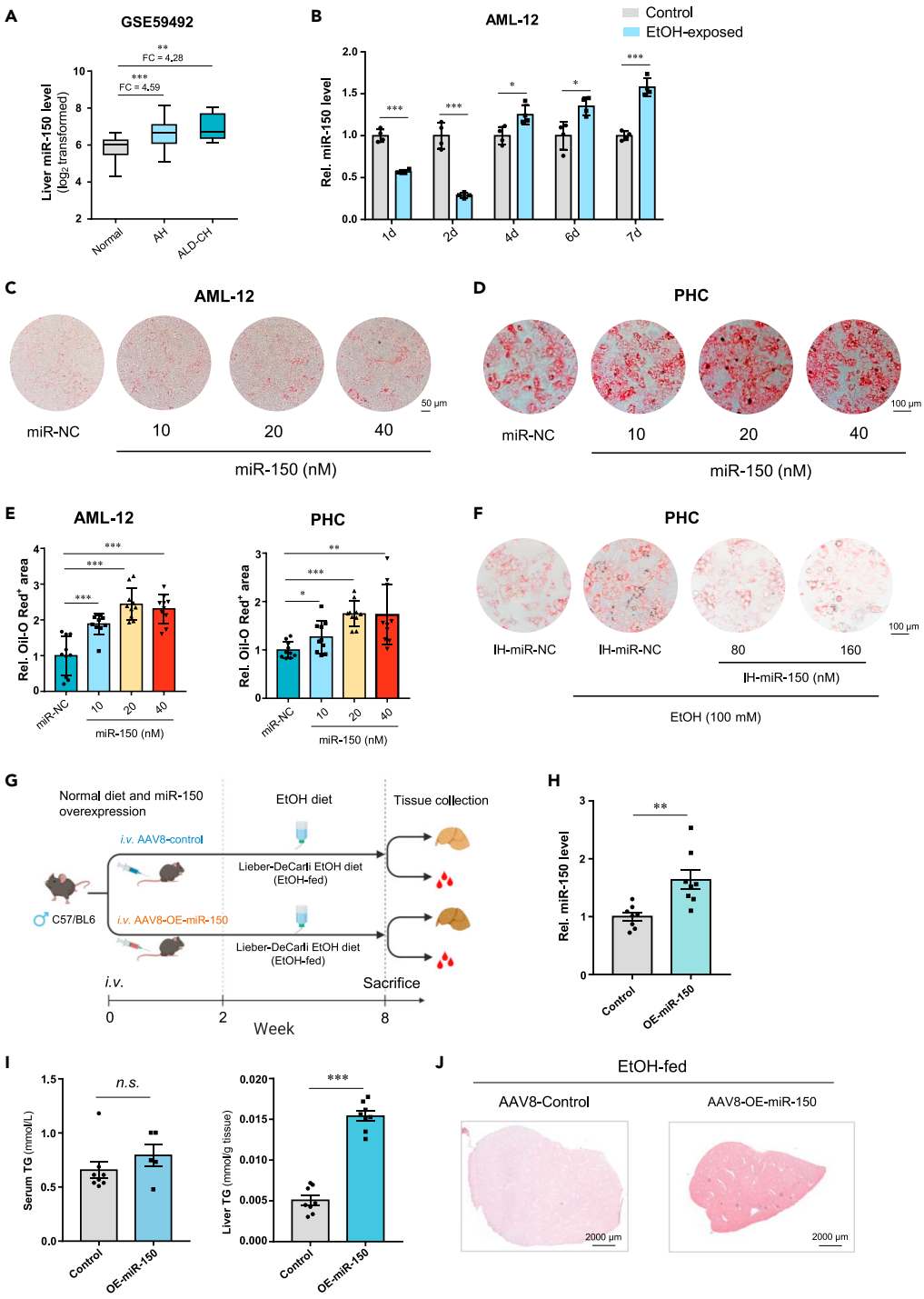

Figure 3. miR-150 increased hepatic lipid accumulation

(A) miR-150 expression levels in the liver tissues of normal individuals and AH and ALD-CH pateints. The expression profiles of miR-150 were retrieved from the GEO database (GEO: GSE59492). Data was shown as mean ± SD. **p < 0.01, ***p < 0.001 as indicated. (B) qRT-PCR analysis of miR-150 expression levels in AML12 cells under different alcohol exposure time. Data was shown as mean ± SD. *p < 0.05, ***p < 0.001 as indicated.

(C and D) Oil Red O staining of AML12 cells (*C*, Scale bar, 50 μM) or mouse PHC (*D*, Scale bar, 100 μM) transfected with 10, 20, and 40 nM miR-150 mimics or control oligonucleotides for 48 h.

(E) Relative Oil Red O positive area measured by ImageJ software. Data was shown as mean ± SD. *p < 0.05, **p < 0.01, ***p < 0.001 as indicated.

(F) Oil Red O staining of mouse PHC exposed to 100 mM ethanol with/without miR-150 inhibitors transfection. Isolated PHC was first transfected with miR-150 inhibitors or control oligonucleotides. After 24 h transfection, PHC was treated with 100 mM ethanol for another 24 h. Scale bar, 100 μM.

Figure 3. *Continued*

(G) Illustration of rAAV administration procedures. Graph was created with BioRender.com.

(H) RT-qPCR analysis of miR-150 expression levels. Data was shown as mean ± SD. **p < 0.01 as indicated.

(I) Serum (left) and liver (right) TG contents in ethanol-fed mice overexpressed miR-150 or not. Data was shown as mean ± SD. *n.s.*, not significant; ***p < 0.001 as indicated.

(J) Liver Oil Red O staining of ethanol-fed mice overexpressed miR-150 or not. Scale bar, 2000 μM. *n.s.*, not significant; *p < 0.05, **p < 0.01, ***p < 0.001 as indicated.

TG levels were not significantly affected. Oil Red O staining corroborated the biochemical data and showed that rAAV-OE-miR-150 indeed exacerbated ethanol-induced liver lipid accumulation (Figure 3J). Collectively, our results indicate that miR-150 is directly involved in the deregulation of lipid homeostasis of AFL.

miR-150 targets *PLIN2* proximal promoter region and upregulates PLIN2 expression

Next, we performed TMT-based quantitative proteomics analysis between livers from E8w+1B mice and pair-fed mice. This approach allows us to capture post-transcriptional regulatory events that may not be captured solely by RNAseq data. Proteins with fold change greater than 1.2 or less than 0.8 ($p < 0.05$) were considered significantly dysregulated (Figure S2A). Further GO enrichment analysis revealed that pathways upregulated in AFL were enriched in fatty acid metabolic process, lipid catabolic process, organic acid catabolic process, etc. (Figure S2A), while downregulated pathways were mainly related to ribose phosphate metabolic process, generation of precursor metabolites and energy, cellular amino acid metabolic process, etc. (Figure S2A). As our data have indicated that miR-150 promoted hepatic lipid accumulation, we therefore investigate whether miR-150 could modulate the expression of genes involved in fatty acid uptake, TG biosynthesis and breakdown (Figure S2B; Table S2).

Nuclear miRNA has been reported to activate or inhibit specific gene expressions by targeting promoters.[26–29] Therefore, we focused on identifying candidate genes that possessed the miR-150 binding sequence motif in the promoter regions (Figure 4A). Among the 35 differentially expressed genes involved in hepatic lipid metabolism, 5 showed a binding site with more than 7 consecutive nucleotides in their promoter regions (sequence 1 kb upstream from the transcription start site, Figure S3A). More importantly, miR-150 significantly increased *PLIN2* mRNA levels in PHC, but hardly affected the expression of *AGPAT2*, *PEX16*, and *ACAA1B* (Figures 4B and 4C). *PEX11A* was not considered as candidate target, because it was a low-expression gene in liver tissues (Figures 4D and S3B), even though *PEX11A* was upregulated by miR-150 (Figure 4C). Taken together, *PLIN2*, a gene involved in lipid sequestration, was selected for further functional and mechanistic studies.

The putative miR-150 binding site in mouse *PLIN2* promoter regions possesses 8 consecutive nucleotides (Figure 4E). Both AML12 cells and PHC treated with miR-150 mimic showed increased PLIN2 expressions at both the mRNA level and protein level (Figures 4F and 4H). Additionally, miR-150 inhibitor was able to inhibit the endogenous expression of PLIN2 (Figures 4G and 4I). To crystallize the functional relationship between miR-150 and it target gene *PLIN2*, isolated hepatocytes was treated with siRNAs against *PLIN2* (Figure 4J). Interestingly, miR-150-induced lipid accumulation in hepatocytes was completely blocked by PLIN2 knockdown (Figure 4K). Our data suggested that PLIN2 was likely a key downstream effector of miR-150 in hepatocytes.

miR-150 directly binds and stabilizes the sense RNA transcripts overlapping the *PLIN2* promoter

Our study has indicated that miR-150 targeted the promoter region of *PLIN2* (Figure 4E). To investigate this further, we employed chromatin isolation by biotinylated RNA pulldown (ChIbRP) assay to study the association between miR-150 and its target chromatin. Specifically, we introduced 3′-biotinylated miR-150 mimics into AML12 cells and, after formaldehyde crosslinking, nuclear fraction isolation, and sonication, the associated chromatin was precipitated. Significant enrichment was observed in the amount of target *PLIN2* DNA, suggesting a strong association between miR-150 and its target chromatin (Figure 5A).

A crucial question that needs to be addressed is whether miR-150 directly binds to genomic DNA. To determine the affinity between miR-150 and single-strand DNA (ssDNA) or double-strand DNA (dsDNA), we synthesized fluorescent-labeled RNA or DNA oligonucleotides and performed *in vitro* fluorescent-based RNA electrophoretic mobility shift assay (FREMSA). Surprisingly, no shift bands were observed in either miR-150/ssDNA mixture (Figure 5B) or miR-150/dsDNA system (Figure 5C), indicating that there was no interaction between miR-150 and its targeted DNA sequence.

Interestingly, we observed a large-scale of H3K27ac, H3K4me1, H3K4me3, and RNA polymeraseII (RNAPII) occupancy signals upstream of the *PLIN2* TSS (Figures 6J and S4A), suggesting that there might be transcripts containing an extended 5′ untranslated region overlapping the *PLIN2* gene promoter, known as promoter-associated RNAs (pRNAs). To confirm their existence and define the 5′ end of the sense pRNAs, we performed a rapid amplification of 5′-cDNA ends (5′-RACE) assay (Figure S4B). As shown in Figure 5D, two similar sense-strand transcripts were observed overlapping the *PLIN2* promoter region. Further quantitative PCR results showed that the sense pRNA transcripts were present at approximately 1.5 copies per primary hepatic cell or 4 copies per AML12 cell (Figure 5E).

To investigate the mechanism by which miR-150 activates *PLIN2*, we conducted experiments to determine whether miR-150 directly binds to the sense-strand *PLIN2* pRNAs. FREMSA results showed a clear motility shift in lane 3 when miR-150 and pRNA oligonucleotides were mixed (Figure 5F), and excessive cold miR-150 probes could competitively bind the pRNA oligonucleotides in lane 4, suggesting the formation of a miRNA/pRNA complex. Thus, our findings indicated that miR-150 preferred to directly bind the sense pRNA transcripts rather than the promoter DNA of *PLIN2*.

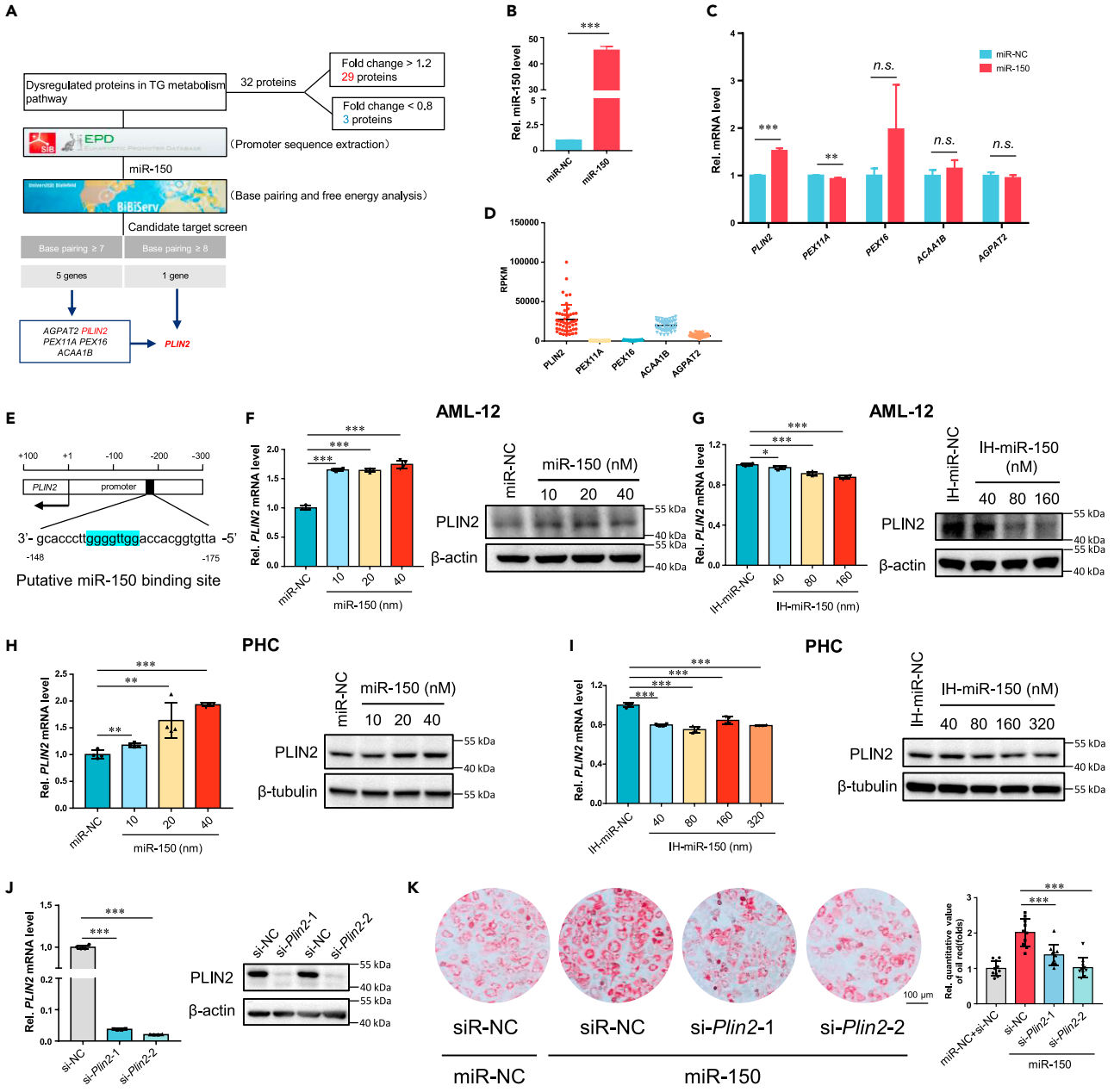

Figure 4. Nuclear miR-150 promotes PLIN2 expressions

(A) Strategy to identify nuclear targets for miR-150 in AFL.

(B and C) qRT-PCR analysis of candidate target genes possibly regulated by miR-150 in mouse primary hepatocytes. Data was shown as mean ± SD. *n.s.*, not significant; **p < 0.01, ***p < 0.001 as indicated.

(D) The hepatic expression levels of candidate target genes in normal human liver tissue. The gene expression profiles were retrieved from TCGA database. Data was shown as mean ± SD.

(E) Schematic illustration of putative binding site of miR-150 in the promoter region of *PLIN2* gene. Base-pairing nucleotides were marked in blue.

(F and G) qRT-PCR and western blotting analysis of PLIN2 expression in AML12 cells transfected with miR-150 mimics (F) or inhibitors (G) for 48 h. Data was shown as mean ± SD. *p < 0.05, ***p < 0.001 as indicated.

(H and I) qRT-PCR and western blotting analysis of PLIN2 expression in mouse primary hepatocytes transfected with miR-150 mimics (H) or inhibitors (I) for 48 h. Data was shown as mean ± SD. **p < 0.01, ***p < 0.001 as indicated.

(J) qRT-PCR and western blotting analysis of the PLIN2 knockdown efficiency in mouse PHC. Data was shown as mean ± SD. ***p < 0.001 as indicated.

(K) Oil Red O staining of PHC co-transfected with miR-150 mimics and/or *PLIN2* siRNAs. Scale bar, 100 μM. ***p < 0.001 as indicated.

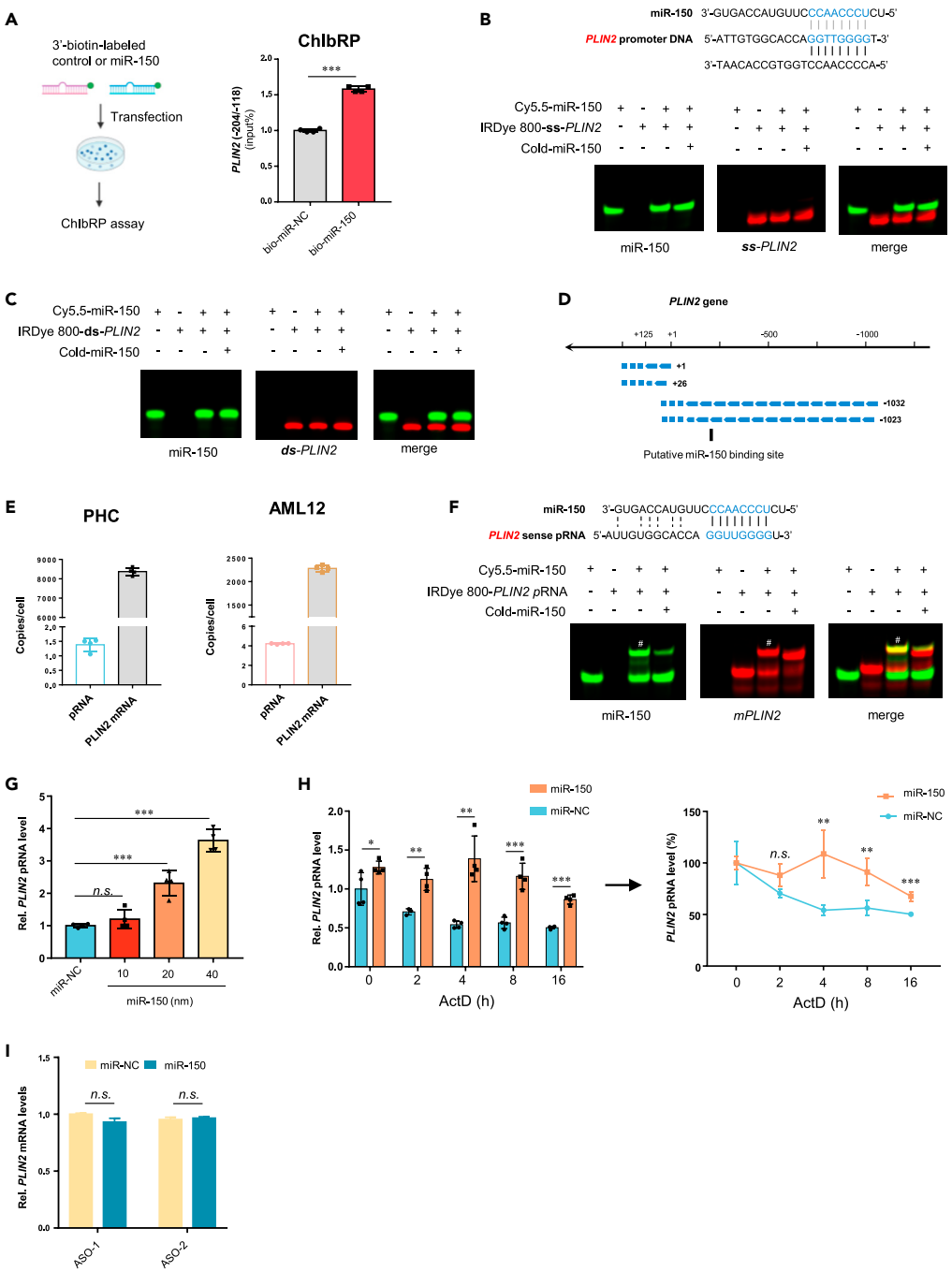

Figure 5. miR-150 directly binds the sense promoter-associated RNA of *PLIN2*

(A) Chromatin isolation by biotinylated RNA pulldown (ChIbRP) analysis of the association between miR-150 and its target chromatin. Data was shown as mean ± SD. ***p < 0.001 as indicated.

(B and C) FREMSA analysis of the interaction between miR-150 and single strand (B) or double strand (C) *PLIN2* promoter DNA.

(D) Schematic illustration of sense transcripts overlapping *PLIN2* promoters identified by 5′-RACE.

(E) qRT-PCR analysis of the copy numbers of sense *PLIN2* pRNAs per cell.

(F) FREMSA analysis of the interaction between miR-150 and sense *PLIN2* pRNA. The number sign # indicates shifted duplex formed by miR-150 and sense pRNA oligonucleotides.

(G) qRT-PCR analysis of the expression levels of sense *PLIN2* pRNA in response to miR-150 treatment. Data was shown as mean ± SD. *n.s.*, not significant; ***p < 0.001 as indicated.

Figure 5. *Continued*

(H) Effect of miR-150 on the RNA stability of *PLIN2* pRNA. Mouse PHC were transfected with miR-150 mimics (20 nM) for 24 h. Then cells were treated with actinomycin D for additional 0, 2, 4, 8, and 16 h, respectively. The pRNA levels were measured by qRT-PCR and normalized by *GAPDH*. Data was shown as mean ± SD. *n.s.*, not significant; *p < 0.05, **p < 0.01, ***p < 0.001 as indicated.

(I) Effect of knocking down sense pRNAs using ASO on the induction of *PLIN2* expression by miR-150 mimics. Data was shown as mean ± SD. *n.s.*, not significant.

Furthermore, we found that miR-150 significantly increased the levels of sense pRNA (Figure 5G). Our further investigations showed that miR-150 transfection inhibited the degradation of sense pRNA (Figure 5H), which likely contribute to the increased sense pRNA levels. To determine the role of sense pRNA in miR-150-induced PLIN2 expression, antisense oligonucleotides (ASOs) were transfected into PHC to reduce the sense pRNA transcript levels (Figure S4C). Our results showed abrogated activation of miR-150 acting on PLIN2 (Figure 5I). Thus, our study suggests that miR-150 promotes PLIN2 expression by directly binding and stabilizing the sense pRNAs.

miR-150 promotes PLIN2 expression by activating transcription

We next aimed to investigate the mechanism by which miR-150 enhances PLIN2 expression in hepatic cells. We found that miR-150 did not affect the degradation of *PLIN2* mRNA (Figure 6A) or primary RNA (Figure S5A). However, we observed a significant increase in *PLIN2* primary RNA levels upon treatment with miR-150 mimics in AML12 cells and PHC (Figure 6B). This led us to hypothesize that miR-150 may promote PLIN2 expression by activating transcription. To test this, we constructed two luciferase reporters with either a 1 kb wild-type promoter sequence or a binding site mutated sequence in the pGL3-basic vector (Figure 6C). Our results showed that miR-150 increased the luciferase activity driven by the wild-type *PLIN2* promoter, while mutation of the predicted binding site abolished this effect (Figure 6D), supporting our hypothesis that miR-150 activates the *PLIN2* promoter.

To determine whether miR-150-induced gene expression was associated with the chromatin accessibility at the *PLIN2* promoter regions, we performed ChIP assay using specific antibodies against histone 3 (H3) modifications. Our results revealed significant modifications of H3K27ac, H3K4me3, and H3K4me1 at the *PLIN2* promoter regions in miR-150 mimic-transfected hepatocytes (Figures 6E and 6F), suggesting an active transcriptional status of the *PLIN2* promoter after miR-150 transfection. Moreover, we examined the binding profiles of different phosphorylated forms of RNAPII upon miR-150 transfection. Our data indicated that miR-150 increased the enrichment of the initiating (non-phosphorylated) form of RNAPII at the *PLIN2* downstream promoter element (Figure 6G). Interestingly, the elongating form of RNAPII with Ser2 phosphorylation at the C-terminal domain (CTD) was found to be drastically enriched on the *PLIN2* gene body (Figure 6H), whereas the paused form of RNAPII with Ser5 phosphorylation was significantly reduced by miR-150 transfection (Figure 6I). Together, our results indicate that miR-150 increases the chromatin accessibility at the *PLIN2* promoter and subsequently stimulates transcription initiation and elongation.

miR-150 facilitates the recruitment of RNAPII and DHX9

The nuclear miRNA/AGO complex has been shown to regulate TGS or activation by targeting the promoter region. In our study, the ChIP-seq signals revealed significant occupancy of AGO2 protein, rather than AGO1, in the proximal promoter region (Figure 6J). Furthermore, ChIP analysis using an antibody specific to AGO2 showed increased binding of AGO2 to the putative miR-150 target site in PHC transfected with miR-150 mimics (Figure 6K). To validate the role of AGO2 in miR-150-induced PLIN2 expression, siRNAs targeting *AGO2* were co-transfected with miR-150 mimics into PHC. Our results showed that knockdown of AGO2 expression abolished the promoting effects of miR-150 on PLIN2 expression (Figures 6L and 6M). These findings indicate that miR-150 targets the *PLIN2* promoter region in an AGO2-dependent manner.

Furthermore, we investigated whether the miR-150-AGO2 complex was associated with RNAPII transcription machinery at the *PLIN2* promoter. We performed co-immunoprecipitation (co-IP) assay from hepatocytes transfected with miR-150 mimics or control oligonucleotides using RNAPII specific antibody. As shown in Figure 6N, basal-level AGO2/RNAPII interactions were observed in control cells, whereas more AGO2 proteins co-immunoprecipitated with RNAPII in miR-150 transfected cells. These data suggest an increased interaction between miR-150-guided AGO2 complex and RNAPII.

DHX9, a transcriptional activator known to recruit general transcriptional machinery to the promoter region, specifically co-immunoprecipitated with AGO2 in miR-150 transfected hepatocytes, whereas minimal association between AGO2 and DHX9 was observed in control cells (Figure 6O). Similarly, DHX9 also co-immunoprecipitated with RNAPII in hepatocytes treated with miR-150 mimic (Figure 6N). Knockdown of DHX9 expression abrogated miR-150-induced PLIN2 expression in PHC (Figure 6P). Taken together, our findings indicate that miR-150-guided AGO2 forms an epigenetic activation complex with RNAPII and DHX9 at the promoter, contributing to increased *PLIN2* transcription.

DISCUSSION

In this study, we showed that miR-150, a nuclear microRNA, was decreased in AFL. Importantly, we found that miR-150 directly interacted with the *PLIN2* pRNAs to recruit the RNAPII transcription machinery to the corresponding promoter region, thereby promoting *PLIN2* transcription. As the lipid droplet-resident protein PLIN2 is known to promote hepatic lipid accumulation, our findings provide a novel compensatory mechanism for the regulation of hepatic lipid homeostasis in alcoholic liver disease.

The subcellular location of biological molecules determines their biological function, thus clarifying the cellular distribution of particular miRNA is a prerequisite for further function and mechanism study. miRNAs are assumed to be active primarily in the cytoplasm, but some

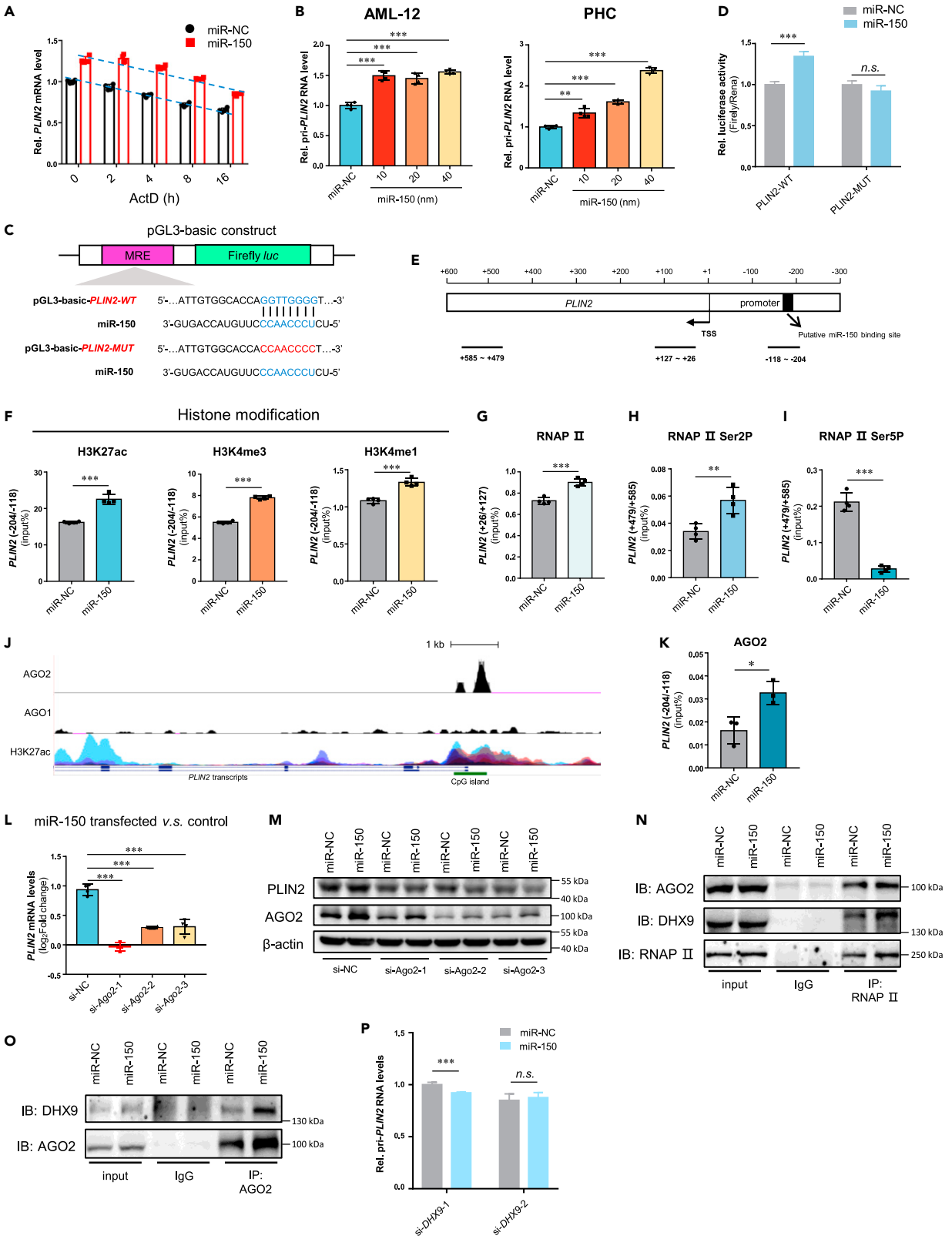
A
miR-NC
miR-150
Rel. PLIN2 mRNA level
ActD (h)
B
AML-12
PHC
Rel. pri-PLIN2 RNA level
miR-150 (nm)
D
miR-NC
miR-150
Rel. luciferase activity (Firefly/Rena)
PLIN2-WT
PLIN2-MUT
n.s.
C
pGL3-basic construct
MRE
Firefly luc
pGL3-basic-PLIN2-WT 5'-…ATTGTGGCACCAGGTTGGGGT…-3'
miR-150 3'-GUGACCAUGUUCCCAACCCUCU-5'
pGL3-basic-PLIN2-MUT 5'-…ATTGTGGCACCACCAACCCCT…-3'
miR-150 3'-GUGACCAUGUUCCCAACCCUCU-5'
E
PLIN2
promoter
TSS
Putative miR-150 binding site
+585 ~ +479
+127 ~ +26
-118 ~ -204
F
Histone modification
H3K27ac
H3K4me3
H3K4me1
PLIN2 (-204/-118) (input%)
G
RNAP II
PLIN2 (+26/+127) (input%)
H
RNAP II Ser2P
PLIN2 (+479/+585) (input%)
I
RNAP II Ser5P
PLIN2 (+479/+585) (input%)
J
1 kb
AGO2
AGO1
H3K27ac
PLIN2 transcripts
CpG island
K
AGO2
PLIN2 (-204/-118) (input%)
L
miR-150 transfected v.s. control
PLIN2 mRNA levels (log2Fold change)
si-NC
si-Ago2-1
si-Ago2-2
si-Ago2-3
M
PLIN2
AGO2
β-actin
55 kDa
40 kDa
100 kDa
N
IB: AGO2
IB: DHX9
IB: RNAP II
100 kDa
130 kDa
250 kDa
input
IgG
IP: RNAP II
O
IB: DHX9
IB: AGO2
130 kDa
100 kDa
input
IgG
IP: AGO2
P
Rel. pri-PLIN2 RNA levels
si-DHX9-1
si-DHX9-2

Figure 6. miR-150 stimulates *PLIN2* transcription

(A) The effect of miR-150 on the RNA stability of *PLIN2* mRNA. Mouse PHC were transfected with miR-150 mimics (20 nM) for 24 h. Then cells were treated with actinomycin D for additional 2, 4, 8, and 16 h, respectively. The *PLIN2* mRNA levels were determined by qRT-PCR and normalized by *GAPDH*.

(B) qRT-PCR analysis of the expression levels of primary *PLIN2* RNA in AML12 cells and mouse PHC transfected with miR-150 mimics for 48 h. Data was shown as mean ± SD. **p < 0.01, ***p < 0.001 as indicated.

(C) Schematic illustration of the luciferase reporter construction that detecting wild-type ang mutated *PLIN2* promoter activities.

(D) The promoter activities measured by the luciferase reporter assay in HEK 293T cells in response to miR-150 mimics. Data was shown as mean ± SD. *n.s.*, not significant; *p < 0.05, **p < 0.01, ***p < 0.001 as indicated.

(E) Graphic illustration of the PCR primer locations in the *PLIN2* promoter after chromatin immunoprecipitation.

(F) ChIP-PCR analysis of the enrichment of H3K27ac, H3K4me1, and H3K4me3 on the proximal promoter containing putative miR-150 target site. Data was shown as mean ± SD. ***p < 0.001 as indicated.

(G–I) ChIP-PCR analysis of the enrichment of non-phosphorylated RNAPII(G) near *PLIN2* TSS, and the occupancy of phosphorylated RNAPII at Ser2 (H) and Ser5 (I) on the *PLIN2* gene body. Data was shown as mean ± SD. **p < 0.01, ***p < 0.001 as indicated.

(J) ChIP-seq profiles of AGO1, AGO2, and H3K27ac across PLIN2 genes. Sequencing tracks were retrieved using the Cistrome Data Browser and visualized by UCSC database.

(K) ChIP-PCR analysis of the enrichment of AGO2 proteins on the proximal promoter containing putative miR-150 target site. Data was shown as mean ± SD. *p < 0.05 as indicated.

(L and M) qRT-PCR and western blotting analysis of PLIN2 expression in mouse PHC co-transfected with miR-150 mimics and AGO2 siRNAs. Data was shown as mean ± SD. ***p < 0.001 as indicated.

(N and O) Co-immunoprecipitation analysis the interaction between AGO2, RNAPII, and DHX9 in response to miR-150 treatment.

(P) qRT-PCR analysis of pri-*PLIN2* expression in mouse PHC co-transfected with miR-150 mimics and DHX9 siRNAs. Data was shown as mean ± SD. *n.s.*, not significant; ***p < 0.001 as indicated.

miRNAs show selective nuclear enrichment.[30] For example, human miR-29b predominantly localizes in the nucleus, whereas its paralog miR-29a is abundant in the cytoplasm. It is demonstrated that the 3′ terminal motif AGUGUU of miR-29b is a transportable nuclear import element that directs the nuclear enrichment of miRNA.[31] The 3′ end sequence of miR-150 is an AGUG motif that may responsible for its nuclear localization, this needs to be confirmed by more investigation in the future.

Compensation is a physiological response that occurs during chemical exposure with the purpose to maintain the body homeostasis.[32] Various miRNAs are dysregulated in response to toxin exposure or disease progression. It is important to determine whether these dysregulations are compensatory responses to adapt injury or toxicological responses to driver damage, because compensatory responses are generally not considered as adverse effects.[33,34] In this study, we found miR-150 was decreased in alcoholic fatty livers, whereas miR-150 showed function to promote hepatic lipid accumulation both *in vitro* and *in vivo*. So miR-150 is decreased as a compensatory response to liver steatosis, and the extent of this response is insufficient to prevent the development of AFL. What's more, we showed that ethanol-induced lipid accumulation can be impaired by exogenous miR-150 inhibitors in isolated PHC. A recent study has reported miR-150 deficiency as protective against Fas-induced liver injury.[35] Based on these findings, we assume that approaches that inhibit miR-150 expression can be potential therapeutics for the treatment of alcoholic liver disease. Further study is required to address this issue.

Interestingly, we found miR-150 regulated hepatic lipid levels by promoting PLIN2 expression. PLIN2 is a member of the lipid droplet coat protein perilipin family which functions as physiological regulator of liver lipid accumulation.[36] PLIN2 is residentially located on the lipid droplet surface and blocks the association of lipases to fat droplets which subsequentially limits TG hydrolysis.[37] In this study, *in vivo* PLIN2 activation was achieved by rAAV8-based miR-150 delivery. rAAV8 serotype vector exerts high affinity to the liver tissue, but the liver exhibits strong heterogeneity. Therefore, we cannot rule out the possibility that miR-150 promotes lipid accumulation by regulating the biological processes of other nonparenchymal cells,[38,39] which needs further investigation.

Although nuclear small RNA-induced TGA is definite, the protein component of the activation effector complex is not clear. In this study, we focused on addressing the mechanism of which miR-150-induced transcriptional *PLIN2* activation. Nuclear miRNAs are generally loaded into Argonaute protein to form an effector complex by recruiting other factors such as chromatin modifiers or RNAP II.[29,40] However, it is still controversial which Argonaute protein is needed for nuclear miRNA-mediated transcriptional gene regulation. At the very beginning, some studies hold the opinion that small noncoding RNAs that modulated TGS were observed to require the participation of AGO1, DNA methyltransferase 3a, and histone deacetylase 1.[41,42] However, later research identified that AGO2 was the primary AGO variant that was recruited to the promoter region during gene activation or silencing.[29,43] Our study provided another evidence that nuclear miRNA-induced TGA depended on AGO2 protein. DHX9, also known as nuclear DNA helicase II, which unwinds both DNA and RNA structures.[44] Recent study unravels that DHX9 acts as a transcriptional activator by recruiting general transcriptional machinery to promoter region.[45–47] Here, we identified that DHX9 interact with AGO2 and facilitate RNAPII recruitment after miR-150 treatment. Still, other components of the effector complex, such as transcription factors, need to be further investigated. And relevant findings will be reported in the future.

Nuclear miRNAs play active regulatory roles through targeting promoter regions or enhancer elements, binding nascent RNA transcripts, or interacting with non-AGO proteins, etc.[23] To date, there is still a very interesting issue that exactly how activating miRNAs recognize and modulate target promoters. Some studies held that miRNAs directly interacted with promoter DNA sequence, but few provided conclusive evidence to prove this viewpoint. More importantly, in this study we used a self-developed RNA EMSA method based on fluorescent

labeling[48] and directly showed that miRNA has poor affinity with DNA oligonucleotides whereas it possesses strong binding capability with corresponding RNA oligonucleotides. This finding suggests that when DNA and its RNA transcripts coexist in the cell, miRNAs preferentially target RNA transcripts. Moreover, several studies have proved that there are RNAPIIexpressed primary RNAs containing an extended 5′ UTR region that overlaps the gene promoter,[26,41,49] thus these pRNAs probably function as recognition elements for activating miRNAs and scaffolds for chromatin modifiers and transcriptional factors. Here we found low-copy sense-strand pRNAs existed in the *PLIN2* proximal promoter region, and demonstrated the pRNA was required for miR-150-directed TGA. We presume that the sense pRNAs may function as scaffolds for miR-150 to bind, allowing the transcription effector complex to be guided directly to the corresponding promoter region of *PLIN2* gene, ultimately driving TGA.

To summarize, our study uncovered a new compensatory response for the homeostasis regulation of ethanol-induced hepatic lipid accumulation. We also identified nuclear miR-150 as a pro-steatosis factor in transcriptionally activating *PLIN2* expression by directly targeting the pRNA. Our findings suggest a potential strategy for the treatment of alcoholic liver disease by inhibiting miR-150.

Limitations of the study

Although our findings demonstrate that the inhibition of miR-150 can reverse ethanol-induced lipid accumulation in PHC, it is necessary to conduct further experimental validation by depleting miR-150 *in vivo* to confirm whether additional miR-150 inhibition can improve liver steatosis in alcoholic liver disease. Another limitation of this study is that we only sequenced the 5′ end of the *PLIN2* pRNAs, and further investigation is required to elucidate the full length sequence of these pRNAs.

STAR★METHODS

Detailed methods are provided in the online version of this paper and include the following:

- KEY RESOURCES TABLE
- RESOURCE AVAILABILITY
  - Lead contact
  - Materials availability
  - Data and code availability
- EXPERIMENTAL MODEL AND SUBJECT DETAILS
  - Cell culture
  - Animal experiments
  - Primary hepatocyte isolation
- METHOD DETAILS
  - Small RNA sequencing and proteomic analysis
  - Prediction of miR-150 nuclear targets
  - RNA purification and qRT-PCR analysis
  - Immunoblotting
  - Luciferase reporter gene assay
  - Cytoplasmic and nuclear fraction isolation
  - miRNA fluorescence *in situ* hybridization (FISH)
  - ChIP assay
  - Chromatin isolation by biotinylated RNA pulldown (ChIbRP) assay
  - RNA stability assay
  - Immunoprecipitation (IP) assay
  - Rapid amplification of cDNA ends (RACE)
  - Fluorescent-based RNA electrophoretic mobility shift assay (FREMSA)
- QUANTIFICATION AND STATISTICAL ANALYSIS

SUPPLEMENTAL INFORMATION

Supplemental information can be found online at https://doi.org/10.1016/j.isci.2023.107837.

ACKNOWLEDGMENTS

We thank Dr. Wen Chen from Sun Yat-sen University for providing the AML12 cells. This work was supported by grants from the National Natural Science Foundation of China (82273670, 91943301, and 81973075).

AUTHOR CONTRIBUTIONS

J.L.: Conceptualization, Investigation, Writing – Original draft, Funding Acquisition. Y.-N.J.: Investigation (lead). N.-N.C.: Resources. G.S.: Investigation. X.N.: Software. S.-Y.Z.: Formal Analysis. D.-K.Y.: Conceptualization, Project Administration, Supervision, Writing – Review & Editing, Funding Acquisition.

DECLARATION OF INTERESTS

The authors declare no competing interests.

Received: June 8, 2023
Revised: July 9, 2023
Accepted: September 2, 2023
Published: September 7, 2023

REFERENCES

1. World Health Organization (2018). Global Status Report on Alcohol and Health. https://www.who.int/substance_abuse/publications/global_alcohol_report/gsr_2018/en/.
2. Gao, B., and Bataller, R. (2011). Alcoholic liver disease: pathogenesis and new therapeutic targets. Gastroenterology *141*, 1572–1585. https://doi.org/10.1053/j.gastro.2011.09.002.
3. Altamirano, J., and Bataller, R. (2011). Alcoholic liver disease: pathogenesis and new targets for therapy. Nat. Rev. Gastroenterol. Hepatol. *8*, 491–501. https://doi.org/10.1038/nrgastro.2011.134.
4. Powell, E.E., Jonsson, J.R., and Clouston, A.D. (2005). Steatosis: co-factor in other liver diseases. Hepatology *42*, 5–13. https://doi.org/10.1002/hep.20750.
5. Seitz, H.K., Bataller, R., Cortez-Pinto, H., Gao, B., Gual, A., Lackner, C., Mathurin, P., Mueller, S., Szabo, G., and Tsukamoto, H. (2018). Alcoholic liver disease. Nat. Rev. Dis. Primers *4*, 16. https://doi.org/10.1038/s41572-018-0014-7.
6. Louvet, A., and Mathurin, P. (2015). Alcoholic liver disease: mechanisms of injury and targeted treatment. Nat. Rev. Gastroenterol. Hepatol. *12*, 231–242. https://doi.org/10.1038/nrgastro.2015.35.
7. Setshedi, M., Wands, J.R., and Monte, S.M.d.l. (2010). Acetaldehyde adducts in alcoholic liver disease. Oxid. Med. Cell. Longev. *3*, 178–185. https://doi.org/10.4161/oxim.3.3.12288.
8. Crabb, D.W., Matsumoto, M., Chang, D., and You, M. (2004). Overview of the role of alcohol dehydrogenase and aldehyde dehydrogenase and their variants in the genesis of alcohol-related pathology. Proc. Nutr. Soc. *63*, 49–63. https://doi.org/10.1079/pns2003327.
9. Clugston, R.D., Yuen, J.J., Hu, Y., Abumrad, N.A., Berk, P.D., Goldberg, I.J., Blaner, W.S., and Huang, L.S. (2014). CD36-deficient mice are resistant to alcohol- and high-carbohydrate-induced hepatic steatosis. J. Lipid Res. *55*, 239–246. https://doi.org/10.1194/jlr.M041863.
10. You, M., Fischer, M., Deeg, M.A., and Crabb, D.W. (2002). Ethanol induces fatty acid synthesis pathways by activation of sterol regulatory element-binding protein (SREBP). J. Biol. Chem. *277*, 29342–29347. https://doi.org/10.1074/jbc.M202411200.
11. Galli, A., Pinaire, J., Fischer, M., Dorris, R., and Crabb, D.W. (2001). The Transcriptional and DNA Binding Activity of Peroxisome Proliferator-activated Receptor α Is Inhibited by Ethanol Metabolism. J. Biol. Chem. *276*, 68–75. https://doi.org/10.1074/jbc.M008791200.
12. Fischer, M., You, M., Matsumoto, M., and Crabb, D.W. (2003). Peroxisome proliferator-activated receptor alpha (PPARalpha) agonist treatment reverses PPARalpha dysfunction and abnormalities in hepatic lipid metabolism in ethanol-fed mice. J. Biol. Chem. *278*, 27997–28004. https://doi.org/10.1074/jbc.M302140200.
13. Puri, V., Konda, S., Ranjit, S., Aouadi, M., Chawla, A., Chouinard, M., Chakladar, A., and Czech, M.P. (2007). Fat-specific Protein 27, a Novel Lipid Droplet Protein That Enhances Triglyceride Storage. J. Biol. Chem. *282*, 34213–34218. https://doi.org/10.1074/jbc.M707404200.
14. Xu, M.J., Cai, Y., Wang, H., Altamirano, J., Chang, B., Bertola, A., Odena, G., Lu, J., Tanaka, N., Matsusue, K., et al. (2015). Fat-Specific Protein 27/CIDEC Promotes Development of Alcoholic Steatohepatitis in Mice and Humans. Gastroenterology *149*, 1030–1041.e6. https://doi.org/10.1053/j.gastro.2015.06.009.
15. Carr, R.M., Peralta, G., Yin, X., and Ahima, R.S. (2014). Absence of perilipin 2 prevents hepatic steatosis, glucose intolerance and ceramide accumulation in alcohol-fed mice. PLoS One *9*, e97118. https://doi.org/10.1371/journal.pone.0097118.
16. Sugimoto, T., Yamashita, S., Ishigami, M., Sakai, N., Hirano, K.i., Tahara, M., Matsumoto, K., Nakamura, T., and Matsuzawa, Y. (2002). Decreased microsomal triglyceride transfer protein activity contributes to initiation of alcoholic liver steatosis in rats. J. Hepatol. *36*, 157–162. https://doi.org/10.1016/s0168-8278(01)00263-x.
17. Jeon, S., and Carr, R. (2020). Alcohol effects on hepatic lipid metabolism. J. Lipid Res. *61*, 470–479. https://doi.org/10.1194/jlr.R119000547.
18. You, M., and Arteel, G.E. (2019). Effect of ethanol on lipid metabolism. J. Hepatol. *70*, 237–248. https://doi.org/10.1016/j.jhep.2018.10.037.
19. Bartel, D.P. (2018). Metazoan MicroRNAs. Cell *173*, 20–51. https://doi.org/10.1016/j.cell.2018.03.006.
20. Heo, M.J., Kim, T.H., You, J.S., Blaya, D., Sancho-Bru, P., and Kim, S.G. (2019). Alcohol dysregulates miR-148a in hepatocytes through FoxO1, facilitating pyroptosis via TXNIP overexpression. Gut *68*, 708–720. https://doi.org/10.1136/gutjnl-2017-315123.
21. Yin, H., Hu, M., Zhang, R., Shen, Z., Flatow, L., and You, M. (2012). MicroRNA-217 promotes ethanol-induced fat accumulation in hepatocytes by down-regulating SIRT1. J. Biol. Chem. *287*, 9817–9826. https://doi.org/10.1074/jbc.M111.333534.
22. Mostofa, M.G., Tran, M., Gilling, S., Lee, G., Fraher, O., Jin, L., Kang, H., Park, Y.K., Lee, J.Y., Wang, L., and Shin, D.J. (2022). MicroRNA-200c coordinates HNF1 homeobox B and apolipoprotein O functions to modulate lipid homeostasis in alcoholic fatty liver disease. J. Biol. Chem. *298*, 101966. https://doi.org/10.1016/j.jbc.2022.101966.
23. Liu, H., Lei, C., He, Q., Pan, Z., Xiao, D., and Tao, Y. (2018). Nuclear functions of mammalian MicroRNAs in gene regulation, immunity and cancer. Mol. Cancer *17*, 64. https://doi.org/10.1186/s12943-018-0765-5.
24. Fan, J., Zhang, X., Nie, X., Li, H., Yuan, S., Dai, B., Zhan, J., Wen, Z., Jiang, J., Chen, C., and Wang, D. (2020). Nuclear miR-665 aggravates heart failure via suppressing phosphatase and tensin homolog transcription. Sci. China Life Sci. *63*, 724–736. https://doi.org/10.1007/s11427-018-9515-1.
25. Chaluvally-Raghavan, P., Jeong, K.J., Pradeep, S., Silva, A.M., Yu, S., Liu, W., Moss, T., Rodriguez-Aguayo, C., Zhang, D., Ram, P., et al. (2016). Direct Upregulation of STAT3 by MicroRNA-551b-3p Deregulates Growth and Metastasis of Ovarian Cancer. Cell Rep. *15*, 1493–1504. https://doi.org/10.1016/j.celrep.2016.04.034.
26. Matsui, M., Chu, Y., Zhang, H., Gagnon, K.T., Shaikh, S., Kuchimanchi, S., Manoharan, M., Corey, D.R., and Janowski, B.A. (2013). Promoter RNA links transcriptional regulation of inflammatory pathway genes. Nucleic Acids Res. *41*, 10086–10109. https://doi.org/10.1093/nar/gkt777.
27. Meng, X., Jiang, Q., Chang, N., Wang, X., Liu, C., Xiong, J., Cao, H., and Liang, Z. (2016). Small activating RNA binds to the genomic target site in a seed-region-dependent manner. Nucleic Acids Res. *44*, 2274–2282. https://doi.org/10.1093/nar/gkw076.
28. Zardo, G., Ciolfi, A., Vian, L., Starnes, L.M., Billi, M., Racanicchi, S., Maresca, C., Fazi, F., Travaglini, L., Noguera, N., et al. (2012). Polycombs and microRNA-223 regulate human granulopoiesis by transcriptional control of target gene expression. Blood *119*, 4034–4046. https://doi.org/10.1182/blood-2011-08-371344.

29. Benhamed, M., Herbig, U., Ye, T., Dejean, A., and Bischof, O. (2012). Senescence is an endogenous trigger for microRNA-directed transcriptional gene silencing in human cells. Nat. Cell Biol. *14*, 266–275. https://doi.org/10.1038/ncb2443.
30. Santovito, D., and Weber, C. (2022). Non-canonical features of microRNAs: paradigms emerging from cardiovascular disease. Nat. Rev. Cardiol. *19*, 620–638. https://doi.org/10.1038/s41569-022-00680-2.
31. Hwang, H.W., Wentzel, E.A., and Mendell, J.T. (2007). A hexanucleotide element directs microRNA nuclear import. Science *315*, 97–100. https://doi.org/10.1126/science.1136235.
32. Matsushita, K., Toyoda, T., Yamada, T., Morikawa, T., and Ogawa, K. (2020). Comprehensive expression analysis of mRNA and microRNA for the investigation of compensatory mechanisms in the rat kidney after unilateral nephrectomy. J. Appl. Toxicol. *40*, 1373–1383. https://doi.org/10.1002/jat.3990.
33. Molina, L.M., Zhu, J., Li, Q., Pradhan-Sundd, T., Krutsenko, Y., Sayed, K., Jenkins, N., Vats, R., Bhushan, B., Ko, S., et al. (2021). Compensatory hepatic adaptation accompanies permanent absence of intrahepatic biliary network due to YAP1 loss in liver progenitors. Cell Rep. *36*, 109310. https://doi.org/10.1016/j.celrep.2021.109310.
34. Ripa, R., Dolfi, L., Terrigno, M., Pandolfini, L., Savino, A., Arcucci, V., Groth, M., Terzibasi Tozzini, E., Baumgart, M., and Cellerino, A. (2017). MicroRNA miR-29 controls a compensatory response to limit neuronal iron accumulation during adult life and aging. BMC Biol. *15*, 9. https://doi.org/10.1186/s12915-017-0354-x.
35. Chen, W., Han, C., Zhang, J., Song, K., Wang, Y., and Wu, T. (2015). miR-150 Deficiency Protects against FAS-Induced Acute Liver Injury in Mice through Regulation of AKT. PLoS One *10*, e0132734. https://doi.org/10.1371/journal.pone.0132734.
36. Libby, A.E., Bales, E., Orlicky, D.J., and McManaman, J.L. (2016). Perilipin-2 Deletion Impairs Hepatic Lipid Accumulation by Interfering with Sterol Regulatory Element-binding Protein (SREBP) Activation and Altering the Hepatic Lipidome. J. Biol. Chem. *291*, 24231–24246. https://doi.org/10.1074/jbc.M116.759795.
37. Listenberger, L.L., Ostermeyer-Fay, A.G., Goldberg, E.B., Brown, W.J., and Brown, D.A. (2007). Adipocyte differentiation-related protein reduces the lipid droplet association of adipose triglyceride lipase and slows triacylglycerol turnover. J. Lipid Res. *48*, 2751–2761. https://doi.org/10.1194/jlr.M700359-JLR200.
38. Zhang, Y., Liu, D., Chen, X., Li, J., Li, L., Bian, Z., Sun, F., Lu, J., Yin, Y., Cai, X., et al. (2010). Secreted monocytic miR-150 enhances targeted endothelial cell migration. Mol. Cell *39*, 133–144. https://doi.org/10.1016/j.molcel.2010.06.010.
39. Selimoglu-Buet, D., Rivière, J., Ghamlouch, H., Bencheikh, L., Lacout, C., Morabito, M., Diop, M., Meurice, G., Breckler, M., Chauveau, A., et al. (2018). A miR-150/TET3 pathway regulates the generation of mouse and human non-classical monocyte subset. Nat. Commun. *9*, 5455. https://doi.org/10.1038/s41467-018-07801-x.
40. Portnoy, V., Lin, S.H.S., Li, K.H., Burlingame, A., Hu, Z.H., Li, H., and Li, L.C. (2016). saRNA-guided Ago2 targets the RITA complex to promoters to stimulate transcription. Cell Res. *26*, 320–335. https://doi.org/10.1038/cr.2016.22.
41. Han, J., Kim, D., and Morris, K.V. (2007). Promoter-associated RNA is required for RNA-directed transcriptional gene silencing in human cells. Proc. Natl. Acad. Sci. USA *104*, 12422–12427. https://doi.org/10.1073/pnas.0701635104.
42. Hawkins, P.G., Santoso, S., Adams, C., Anest, V., and Morris, K.V. (2009). Promoter targeted small RNAs induce long-term transcriptional gene silencing in human cells. Nucleic Acids Res. *37*, 2984–2995. https://doi.org/10.1093/nar/gkp127.
43. Chu, Y., Yue, X., Younger, S.T., Janowski, B.A., and Corey, D.R. (2010). Involvement of argonaute proteins in gene silencing and activation by RNAs complementary to a non-coding transcript at the progesterone receptor promoter. Nucleic Acids Res. *38*, 7736–7748. https://doi.org/10.1093/nar/gkq648.
44. Zhang, S., and Grosse, F. (1994). Nuclear DNA helicase II unwinds both DNA and RNA. Biochemistry *33*, 3906–3912. https://doi.org/10.1021/bi00179a016.
45. Ren, X., Wang, D., Zhang, G., Zhou, T., Wei, Z., Yang, Y., Zheng, Y., Lei, X., Tao, W., Wang, A., et al. (2023). Nucleic DHX9 cooperates with STAT1 to transcribe interferon-stimulated genes. Sci. Adv. *9*, eadd5005. https://doi.org/10.1126/sciadv.add5005.
46. Liu, S., He, L., Wu, J., Wu, X., Xie, L., Dai, W., Chen, L., Xie, F., and Liu, Z. (2021). DHX9 contributes to the malignant phenotypes of colorectal cancer via activating NF-kappaB signaling pathway. Cell. Mol. Life Sci. *78*, 8261–8281. https://doi.org/10.1007/s00018-021-04013-3.
47. Huo, L., Wang, Y.N., Xia, W., Hsu, S.C., Lai, C.C., Li, L.Y., Chang, W.C., Wang, Y., Hsu, M.C., Yu, Y.L., et al. (2010). RNA helicase A is a DNA-binding partner for EGFR-mediated transcriptional activation in the nucleus. Proc. Natl. Acad. Sci. USA *107*, 16125–16130. https://doi.org/10.1073/pnas.1000743107.
48. Yu, D., Chen, S., Li, D., Knox, B., Guo, L., and Ning, B. (2020). FREMSA: A Method That Provides Direct Evidence of the Interaction between microRNA and mRNA. Methods Mol. Biol. *2102*, 557–566. https://doi.org/10.1007/978-1-0716-0223-2_30.
49. Singh, I., Contreras, A., Cordero, J., Rubio, K., Dobersch, S., Günther, S., Jeratsch, S., Mehta, A., Krüger, M., Graumann, J., et al. (2018). MiCEE is a ncRNA-protein complex that mediates epigenetic silencing and nucleolar organization. Nat. Genet. *50*, 990–1001. https://doi.org/10.1038/s41588-018-0139-3.
50. Luo, J., Hou, Y., Ma, W., Xie, M., Jin, Y., Xu, L., Li, C., Wang, Y., Chen, J., Chen, W., et al. (2021). A novel mechanism underlying alcohol dehydrogenase expression: hsa-miR-148a-3p promotes ADH4 expression via an AGO1-dependent manner in control and ethanol-exposed hepatic cells. Biochem. Pharmacol. *189*, 114458. https://doi.org/10.1016/j.bcp.2021.114458.

STAR★METHODS

KEY RESOURCES TABLE

REAGENT or RESOURCE	SOURCE	IDENTIFIER
Antibodies		
Anti-PLIN2 antibodies	Abcam	Cat# ab108323; RRID: AB_10863476
Anti-Ago1 antibody	Abcam	Cat# ab5070; RRID:AB_2277644
Anti-Ago2 antibody	Abcam	Cat# ab156870; RRID: AB_2687492
Anti-Argonaute-2 antibody (for ChIP)	Abcam	Cat# ab57113; RRID: AB_2230916
Anti-β-Actin Antibody	Boster	Cat# BM0627; RRID: AB_2814866
Anti-Beta Tubulin Antibody	Boster	Cat# M01857-3
Anti-Histone H3 (acetyl K27) antibody (for ChIP)	Abcam	Cat# ab177178; RRID: AB_2828007
Anti-Histone H3 (mono methyl K4) antibody (for ChIP)	Abcam	Cat# ab8895; RRID: AB_306847
Anti-Histone H3 (tri methyl K4) antibody (for ChIP)	Abcam	Cat# ab8580; RRID: AB_306649
Anti-RNA polymerase II antibody (for ChIP)	Abcam	Cat# ab264350
Recombinant Anti-RNA polymerase II CTD repeat YSPTSPS (phospho S2) antibody (for ChIP)	Abcam	Cat# ab238146
Anti-RNA polymerase II CTD repeat YSPTSPS (phospho S5) antibody	Abcam	Cat# ab5408; RRID: AB_304868
Chemicals, peptides, and recombinant proteins		
Certified Fetal Bovine Serum (FBS)	VivaCel	C04001500
Collagenase IV	Gibco BRL	9001-12-1
Dexamethasone	Sigma-Aldrich	D4902
Dynabeads® MyOne Streptavidin C1	Invitrogen	65001
Dynabeads® protein A/G magnetic beads	Invitrogen	80104G
HiScript® III RT SuperMix	Vazyme Biotech Co., Ltd	R323-01
High-glucose DMEM	Basal Media	L110KJ
ITS-G	Gibco BRL	41400045
L-glutamine,	Basal Media	S240JV
Lipofectamine RNAiMAX	Invitrogen	13778-150
Penicillin-streptomycin	Basal Media	S110JV
Percoll	GE Healthcare	17089109
Proteinase K	Thermo Fisher Scientific	00866069
QuantiNova™ SYBR Green PCR reagent	QIAGEN	208054
William E medium	Basal Media	L660KJ
RIPA lysis buffer	Thermo Fisher Scientific	89900
RNAiso Plus reagent	Takara	9109
Rnase A	Thermo Fisher Scientific	00865872
Rabbit IgG	Beyotime	Cat# A7016; RRID: AB_2905533
Critical commercial assays		
Dual Luciferase Reporter Assay Kit	Vazyme Biotech Co., Ltd	DL101-01
HiScript®-TS 5′/3′ RACE Kit	Vazyme Biotech Co., Ltd	RA101

(*Continued on next page*)

Continued

REAGENT or RESOURCE	SOURCE	IDENTIFIER
LightShift Chemiluminescent RNA EMSA Kit	Thermo Fisher Scientific	20158
miRNA 1st Strand cDNA Synthesis Kit	Vazyme Biotech Co., Ltd	MR101
PARIS kit	Invitrogen	AM1921
miRNA FISH Kit	GenePharma	N/A
Experimental models: Cell lines		
Mouse AML-12	Laboratory of Dr. Wen Chen	N/A
Mouse primary hepatocytes	male C57BL/6J mice	N/A
Experimental models: Organisms/strains		
Male C57BL/6JNifdc mice	Charles River	https://www.vitalriver.com/#/animalModel/detailedReading?id=21&namecode=strain
Lieber-DeCarli diet	Readydietech Co., Ltd	L10016A
Oligonucleotides		
miR-150 mimics	Dharmacon	N/A
miR-150 inhibitors	Qiagen	N/A
siRNAs	GenePharma	N/A
ASO	GenePharma	N/A
Primers for qPCR, see Table S3	This paper	N/A
Primers for 5′-RACE, see Table S4	This paper	N/A
Oligonucleotides for 5′-RACE, see Table S5	This paper	N/A
Recombinant DNA		
Plasmid: pGL3-basic-PLIN2-WT	This paper	N/A
Plasmid: pGL3-basic-PLIN2-MUT	This paper	N/A
rAAV8-OE-miR-150	This paper	N/A
Software and algorithms		
GraphPad Prism 7.00	GraphPad	http://www.graphpad.com/; RRID: SCR_002798
Image J	Image J	https://imagej.net ; RRID: SCR_003070

RESOURCE AVAILABILITY

Lead contact

Further information and requests for resources and reagents should be directed to and will be fulfilled by the Lead Contact, Dr. Dianke Yu (dianke.yu@qdu.edu.cn).

Materials availability

All unique materials generated in this study are available from the lead contact upon completion of materials transfer agreement with Qingdao University.

Data and code availability

- All data reported in this paper will be shared by the lead contact upon reasonable request.
- This paper does not report original code.
- Any additional information required to reanalyze the data reported in this paper is available from the lead contact upon request.

EXPERIMENTAL MODEL AND SUBJECT DETAILS

Cell culture

Mouse liver normal cell line AML12 was a gift from Professor Wen Chen (School of Public Health, Sun Yat-sen University) and culture in DMEM medium supplemented with 10% FBS, 1% ITS-G, and 40 ng/ml dexamethasone. Primary hepatocytes were cultured in William E medium containing 10% FBS, 1% L-glutamine, 1% ITS-G, 1% Penicillin-streptomycin, and 5 nM dexamethasone. Cells were transfected with miR-150

mimics, inhibitors, or siRNAs/ASO (Table S6) at specified concentrations using Lipofectamine RNAiMAX for 48 h according to the manufacturer's instructions.

Animal experiments

Eight- to ten-week-old male C57BL/6J mice were purchased from Charles River (Beijing, China) and housed under controlled temperature (24 ± 2°C) and humidity (50–60%) with a regular 12/12-h light/dark cycle. All animal experiments were approved by the Animal Care and Use Committee of Qingdao University. Mice were subjected to several chronic-plus-binge ethanol feeding protocols. First, to adapt mice to liquid diet, all mice were fed on a control Lieber-DeCarli diet *ad libitum* for 5 days. Then ethanol-fed mice were allowed free access to the liquid diet containing 4% (w/w) ethanol for 10 days, 6 weeks, or 8 weeks. On the last day of the experiment, ethanol-fed mice received a single dose of ethanol (5 g/kg body weight) by gavage in the early morning and sacrificed 9 h later. Pair-fed mice were fed with the control liquid diet, followed by isocaloric dextrin-maltose gavage.

For rAAV administration, mice were divided into rAAV8-OE-miR-150 group and rAAV8-control group. rAAV8 systems were delivered into mice by tail vein injection. After 2 weeks, all mice were further fed with Lieber-DeCarli diet containing 4% (w/w) ethanol for another 6 weeks.

Primary hepatocyte isolation

Primary hepatocytes were isolated from six- to eight-week-old C57/BL6J mice. After anesthesia, mice were cannulated from the inferior vena cava, and the liver was perfused and digested with collagenase IV buffer solution. The liver was then dissected, minced, and filtered through a 70 μm cell strainer. Then, hepatocytes were separated by centrifugation. Finally, hepatocytes are purified by density-based separation using Percoll solution.

METHOD DETAILS

Small RNA sequencing and proteomic analysis

Small RNA sequencing and analysis were performed by OE Biotech Co., Ltd. (Shanghai, China). 1 μg total RNAs from E8w+1B mice and pair-fed mice (n = 5) were subjected to the small RNA library construction using the TruSeq Small RNA Sample Prep Kits (Illumina, USA). Qualified libraries were finally sequenced using the Illumina HiSeq X Ten platform. miRNAs with the threshold of $|\log2FC| > 0.58$ and $p < 0.05$ were considered significantly dysregulated.

TMT quantitative proteome was conducted and analyzed by Shanghai Applied Protein Technology Co., Ltd. (Shanghai, China). Total proteins were extracted from the livers of E8w+1B mice and pair-fed mice with 6 biological replicates, followed by protein digestion by trypsin according to the filter-aided sample preparation (FASP) procedure. 100 μg peptide mixture of each sample was labeled using TMT reagent (Thermo Scientific) according to the manufacturer's instructions. Labeled peptides were then fractionated by High pH Reversed-Phase Peptide Fractionation Kit (Thermo Scientific) and subsequentially subjected to LC-MS/MS analysis using a Q Exactive mass spectrometer coupled to Easy nLC (Thermo Scientific). Proteins were identified and quantified by searching the MS raw data using the MASCOT engine (Matrix Science, London, UK; version 2.2) embedded into Proteome Discoverer 1.4 software. Differently expressed proteins were filtered with the criteria of Fold change > 1.3 and $p < 0.05$.

Prediction of miR-150 nuclear targets

The promoter sequences (1 kb upstream from the transcription start site) of 32 differently expressed proteins involved in AFL hepatic lipid metabolism were obtained from the EPD database (https://epd.epfl.ch//index.php). RNAhybrid algorithm (http://bibiserv2.cebitec.unibielefeld.de/rnahybrid) was applied for miR-150 target prediction, and genes possessed base-pairing at least 7 consecutive nucleotides with miR-150 seed region were considered as putative targets.

RNA purification and qRT-PCR analysis

Total RNA was extracted using RNAiso Plus reagent. Total RNA was reverse-transcribed into 1st cDNA using HiScript III RT SuperMix. For small RNA transcription, total RNA was reverse-transcribed with the miRNA 1st Strand cDNA Synthesis Kit using stem-loop primers. Quantitative real-time PCR was performed with QuantiNova™ SYBR Green PCR reagent based on the LightCycler® 480 System (Roche, Basel, Switzerland). Primers used in this study were listed in Table S3.

Immunoblotting

Cells were lysed with RIPA lysis buffer. And protein samples were then separated on 8–10% SDS-PAGE gel, and transferred to polyvinylidene fluoride membrane. After incubation with primary antibodies overnight at 4°C, the specific protein was detected by incubation with corresponding secondary antibodies and visualized by using the ECL western blotting substrate.

Luciferase reporter gene assay

First, the recombinant reporter plasmid was constructed by inserting the wild-type promoter sequence (1 kb upstream of the TSS of *PLIN2* gene) or a seed site mutated one into the pGL3-basic vector. Then the recombinant reporter and pRL-SV40 plasmid were co-transfected into

HEK293 FT cells with or without miR-150 mimics treatment. After 48 h incubation, the Firefly luciferase activity was measured using the Dual-Luciferase Reporter Assay Kit and normalized to the Renilla luciferase value.

Cytoplasmic and nuclear fraction isolation

The cytoplasmic and nuclear fractions of AML12 cells or primary hepatocytes were isolated using the PARIS kit as we described previously.[50] The total RNAs were extracted from the isolated fractions and miRNAs distribution was determined by qRT-PCR. The fold enrichment was calculated by the 2^{-dCt} method.

miRNA fluorescence *in situ* hybridization (FISH)

miR-150 FISH was performed using the RNA FISH Kit from GenePharma. Mouse primary hepatocytes were plated on a slide in 24-well plate. After overnight culture, cells were fixed with 4% paraformaldehyde, followed by cell permeation with 0.1% Triton X-100. Then cell slide was immersed in 2×SSC buffer and incubated in a hybridization solution containing miR-150 detecting probes at 37°C overnight. The probes were pre-treated by heating at 73°C for 5 min to denaturation. After extensive washing, cell slide was treated with DAPI solution for nuclear staining. Images were captured by a Leica confocal microscope.

ChIP assay

Cells were crosslinked with 1% formaldehyde, and then the nuclei were isolated and harvested in lysis buffer containing 1% SDS. Sonicated and diluted lysates were incubated with specific antibodies against H3K27ac, H3K4me3, H3K4me1, AGO2, RNAPII, RNAPII Ser2, and RNAPII Ser5 (Abcam) at 4°C overnight. Then the immunocomplexes were enriched on the Dynabeads® protein A/G magnetic beads. After multiple washes with Low-Salt wash buffer, High-Salt wash buffer, LiCl wash buffer, and TE buffer, the immunocomplexes were eluted, reverse-cross-linked, and digested by proteinase K and Rnase A. Finally, the DNA enrichment level was determined by real-time PCR. Primers used in ChIP-PCR was listed in Table S3.

Chromatin isolation by biotinylated RNA pulldown (ChIbRP) assay

The ChIbRP assay was performed based on the standard ChIP protocol as described above. AML12 cells were transfected with 3′-biotinylated miR-150 mimics for 48 h. Subsequentially, cells were cross-linked, washed, and fractioned, and the nuclei pellet was lysed using the lysis buffer containing 10 Mm EDTA and 1% SDS. After sonication using Bioruptor with the condition of 3 cycles of 30s on and 30 s off, the nuclear lysates were incubated with Dynabeads® MyOne Streptavidin C1 (Invitrogen) overnight. After multiple washes, the beads were resuspended in the elution buffer (100 mM Tris pH 8.0, 10 mM EDTA, 1% SDS) and incubated at 65°C for 5 min. The eluted samples were then de-crosslinked and treated with Rnase A and proteinase K. miR-150 associated DNA was then purified and quantified by real-time PCR using the primers flanking its target site.

RNA stability assay

Primary hepatocytes were transfected with miR-150 mimics for 24 h. Actinomycin D was then added to the culture medium at the concentration of 5 μg/ml, and treated cells were harvested after another 2, 4, 8, and 16 h incubation. Corresponding RNA levels were then quantified by qRT-PCR, and *GAPDH* was used as the internal reference gene.

Immunoprecipitation (IP) assay

Primary hepatocytes were transfected with miR-150 mimics (40 nM) or control oligonucleotides for 48 h. On the day of IP, cells were lysed with NETN buffer (50mM Tris pH 8.0, 150mM NaCl, 1Mm EDTA, 1% NP40), and 0.5 mg total proteins were incubated with corresponding antibodies at 4°C overnight. Then protein A/G magnetic beads were added to the IP system and incubated for another 2 h at 4°C. After multiple washes with NETN buffer, the immunocomplexes were eluted in 2X SDS loading buffer by boiling at 95°C for 5 min. Finally, the eluted proteins were analyzed by immunoblotting.

Rapid amplification of cDNA ends (RACE)

5′-RACE was performed using the HiScript-TS 5′/3′ RACE Kit according to the manufacturer's instructions. In brief, 1 μg total RNA from primary hepatocytes was first reverse-transcribed by reverse transcriptase with template-switching activity using random primers, and then the 5′ end of the cDNA was amplified using high-fidelity DNA polymerase and a set of 5′ gene specific primers (GSP). The PCR products were analyzed on the 1% agarose gel, then major PCR bands were purified, cloned to the T Vector, and sequenced by Sanger sequencing. The sequences of 5′GSPs were listed in Table S4.

Fluorescent-based RNA electrophoretic mobility shift assay (FREMSA)

FREMSA was performed according to our previously published work. IRDye Light® 800 labeled miR-150 oligonucleotides, Cy5.5™ labeled *PLIN2* pRNA oligonucleotides, Cy5.5™ labeled *PLIN2* sense-strand DNA oligonucleotides and unlabeled miR-150 oligonucleotides, unlabeled *PLIN2* antisense-strand DNA oligonucleotides were synthesized by Takara (Dalian, China). To detect the interaction between

miR-150 and *PLIN2* pRNA or the interaction between miR-150 and single-strand *PLIN2* DNA oligonucleotides, labeled miR-150 and pRNA or ssDNA oligonucleotides were incubated in a buffer containing 1 × RNA EMSA binding buffer (Thermo), 5% glycerol, 200 mM KCl, and 100 mM $MgCl_2$ at 25°C for 20 min. Finally, the reaction products were separated on a 12% native PAGE and detected by the Odyssey CLxInfrared Imaging System (Lincoln, NE, USA). Cold miR-150 oligonucleotides were used for competition assay at 50-fold excess.

To detect the interaction between miR-150 and double-strand *PLIN2* DNA oligonucleotides, Cy5.5™ labeled *PLIN2* sense strand DNA oligonucleotides and unlabeled *PLIN2* antisense strand DNA oligonucleotides were first mixed at 1:1 molar, heated in 1× NEB buffer 2 at 95°C for 5 min, and then slowly cooled down at room temperature for 20 min to generate the double strand *PLIN2* DNA fragments. Then labeled miR-150 oligonucleotides and ds*PLIN2* DNA fragments were incubated in the reaction buffer at 60°C for 1 hr, and the reaction products were detected using Odyssey CLxInfrared Imaging System. The sequences of oligonucleotides used in this study were listed in Table S5.

QUANTIFICATION AND STATISTICAL ANALYSIS

All statistical analyses were performed using GraphPad Prism7 software. All data in this study were presented as the mean ± SD from at least three independent experiments. Differences were analyzed by Student's T-test or one-way ANOVA as appropriate. $p < 0.05$ was considered significant (*$p < 0.05$, **$p < 0.01$, and ***$p < 0.001$).